Performance Simulation of a Quadrupole Mass Filter Operating in the First and Third Stability Zones

Thomas J. Hogan and Stephen Taylor

***Abstract*—A method of computation that accurately simulates the performance of quadrupole mass filters (QMFs) is described. Behavior is described by determining the individual trajectories of a large number of ions (10^8) as they are injected into the QMF. The effects of the ratio of circular electrode radius r to electric field radius $r0$ on the performance characteristics have been investigated for zone 1 ($a \approx 0.237$ and $q \approx 0.706$) and zone 3 ($a \approx 3.16$ and $q \approx 3.23$) operation. We demonstrate that performance sensitivity to the $r/r0$ ratio is different for zone 3 than those previously reported for zone 1. The magnitude and variation of the "tail" in the mass spectral peak shapes that are apparent for zone 1 is much decreased for zone 3 and does not influence QMF resolution. Variation in ion trajectories and associated power-spatial frequency spectra when operated in zones 1 and 3 with varying $r/r0$ geometrical ratios are also presented. We demonstrate that these provide an alternative method in determining an ideal value for $r/r0$.**

***Index Terms*—Mathieu stability regions, multipoles, power frequency spectrum, quadrupole mass filter (QMF), spatial frequencies.**

I. Introduction

QUADRUPOLE mass analyzers separate ions according to their mass to charge (m/z) ratio and are a vital component of quadrupole mass spectrometers (QMSs) that provide the selective filtering that is necessary to separate the constituent components of the sample under analysis. Ion trap [1], [2], time of flight, and quadrupole mass filter (QMF) are all types of mass analyzers providing differing performance and operational characteristics. Attributes of the QMF have ensured that it has been deployed in a wide range of applications from modest residual gas analyzers to high-end mass spectrometers for molecular analysis. The characteristics that have ensured its widespread use include relatively simple mechanical construction, simple drive requirements, acceptable power consumption, and a linear mass scale. Modern process control and scientific instrument designers are under constant pressure to increase performance while simultaneously decreasing power consumption and physical size. The mechanical characteristics of the QMF make it suitable for miniaturization through the use of microengineered mechanical system (MEMS) techniques, providing a simultaneous reduction in operating voltage and power budget. The use of these techniques may require more novel geometries to be developed. Previously reported examples of miniature mass filters include [3]–[5].

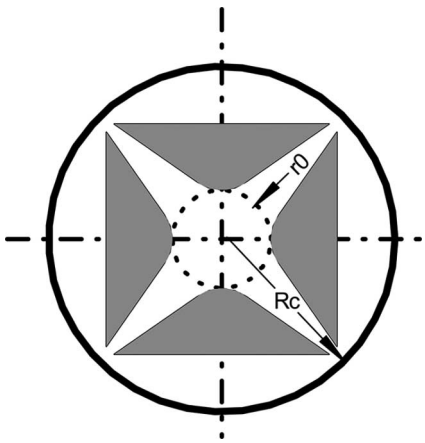

Fig. 1. End view of the QMF that is constructed from hyperbolic-shaped electrodes with field radius $r0$ and case radius Rc.

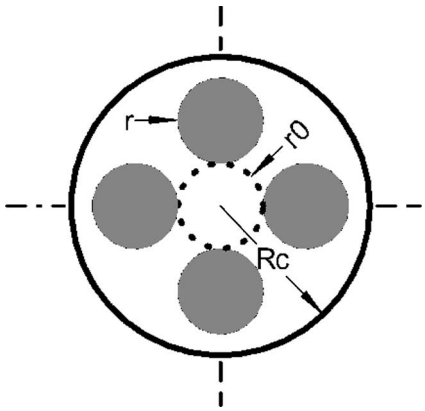

Fig. 2. End view of the QMF that is constructed from circular electrodes with electrode radius r, field radius $r0$, and case radius Rc.

For the QMS, ideal performance is obtained when the QMF is constructed from hyperbolic-shaped rods (Fig. 1) that are perfectly aligned. In practice, most commercial QMFs are manufactured from circular section electrodes (rods) for reasons of cost and ease of manufacture (Fig. 2), resulting in electric fields that deviate from the ideal. Stability zone 1 ($a \approx 0.23$ and $q \approx 0.7$) is the normal operating region for most commercial QMSs [6]. There are, however, advantages of mass spectral peak shape, decreased evidence of low-mass "tails," and increased resolution to be gained from operation in the third

Manuscript received January 11, 2007; revised June 21, 2007.

The authors are with the Department of Electrical Engineering and Electronics, University of Liverpool, L69 3GJ Liverpool, U.K. (e-mail: t.j.hogan@liverpool.ac.uk; s.taylor@liverpool.ac.uk).

Color versions of one or more of the figures in this paper are available online at http://ieeexplore.ieee.org.

Digital Object Identifier 10.1109/TIM.2007.911632

stability zone ($a \approx 3.16$ and $q \approx 3.23$). Zone 3 requires higher operating voltages, which have previously been seen as a disadvantage. With the introduction of much smaller (miniaturized) QMFs, the increased voltage budget may not currently be considered as a technical or economic barrier.

Since the extensive early work of Dawson [6], numerical computer simulation techniques have been employed to investigate the theoretical performance of QMFs. Examples of this work for hyperbolic rods include the effects of RF frequency, phase, and magnitude on QMF performance [7]; the effects of aperture and harmonics on ion transmission [8]; and the effects of aperture parameters and finite length on transmission [9]. Later research undertook a detailed computer simulation of mass spectra for both hyperbolic and circular rods [10], [11]. More recently, computer simulation has been used to investigate the effect of varying the ratio of round-rod radius r to field radius $r0$, which is referred to as $r/r0$. Originally, empirical work [12] applied to the fields that are produced by magnetic pole faces identified 1.148 as the optimum value for this ratio, which results in the dodecapole $(A6)$ multipole field coefficient equating to zero. For a number of years, the requirement for the dodecapole term to be zero was considered to provide optimum performance, albeit the exact value has been refined by later researchers [13], [14]. Later it was concluded [15] that the performance of a QMF could be improved by selecting a value of $r/r0$ that produced approximately equal and opposite A_6 and A_{10} multipole coefficients, resulting in reduced nonlinear resonances. More recently, the use of computed mass spectra for a large number of ions has demonstrated that equating the dodecapole (A_6) term to zero does not provide an optimum QMF performance. Gibson and Taylor [16], [17] used computed spectra for hyperbolic and round-rod QMFs to investigate zone 1 performance under a number of operating conditions. These results quantify the degradation in performance that occurs when operating with nonoptimum values of $r/r0$. They suggested that the optimum performance may not occur when the dodecapole (A_6) term is zero. Simulation results identified an optimum setting for an $r/r0$ of 1.120–1.130. At this ratio, maximum resolution and minimum low-mass tail were obtained. The aforementioned findings were explained in terms of field multipole coefficients [18] and confirmed that selecting $r/r0$ to obtain a dodecapole (A_6) coefficient $= 0$ does not produce optimum QMF performance. Also, the previous result of $r/r0 = 1.120{-}1.130$ was confirmed, producing optimum performance and corresponding to a nonzero value for the dodecapole (A_6) coefficient. This optimum performance is achieved because the A_6 and A_{10} multipole coefficients are of similar magnitude and opposite sign, thereby partially canceling out each other. It is now widely accepted that a value of $\approx$1.127 provides optimum performance when operating in stability zone 1.

Operation in stability zone 3 results in a reduced QMF acceptance area compared to stability zone 1 [19], with a greater acceptance in the x-axis than in the y-axis. This suggests that zone 3 operation may exhibit differing $r/r0$ performance sensitivities due to the variations in the field area that the ions experience. This was a motivation for this investigation. Simulations of mass spectra with a large number of ions (2×10^5) at each mass step are computationally intensive, requiring 24 h or more on a high-end PC. A faster method of identifying optimum electrode geometry is a useful tool. Previously published results [18] introduced the concept of offsetting or canceling multipole coefficients as a method of identifying optimum $r/r0$ ratio. For the fourfold symmetric case of four circular rods, this is relatively straightforward. The use of MEMS-type construction techniques to realize miniature QMFs is of considerable interest. When using this type of construction technique, the resultant electrostatic field is dependent not only on the rod geometry but also on the electrical properties (i.e., dielectric constant) of the surrounding material. A more complex relationship between the physical implementation and the resultant field now exists. This may require different electrode geometries to achieve optimum performance. We therefore seek an alternative and speedier approach for the assessment of QMF performance.

Here, we report on mass spectra that are obtained through computer simulation using our custom software packages (QMS2D-Hyperbolic, QMS2D-Field, and public domain software Poisson/Superfish [20]) on the effects of $r/r0$ on QMF performance when operating in stability zone 3. Results indicate that zone 3 performance characteristics are dependent on $r/r0$, but to a lesser degree than that for zone 1 operation. We also introduce the use of ion trajectory power frequency spectra as a method for the identification of an optimum value for $r/r0$. Results demonstrate that this method provides an accurate and much speedier identification of ideal electrode geometry when compared to mass spectra simulations. With a suitable electrode geometry identified, more detailed QMF performance characteristics can be derived using high-ion-count mass spectra simulations.

II. Theory

Fig. 1 shows an end view of a QMF constructed from four hyperbolic rods that are arranged to produce a radial aperture of radius $r0$ between the pole tips and located in a grounded circular enclosure of radius Rc. When a potential of $+\Phi_A$ is applied to the pair of x rods and a potential of $-\Phi_A$ is applied to the pair of y rods, the generated electric potential in the aperture can be defined by (1), where x and y define the position in the field radius

$$\Phi(x, y) = \frac{\Phi_A(x^2 - y^2)}{2r_0^2}. \tag{1}$$

This field consists of a quadrupole term, resulting in an electric field that linearly increases from the axis center and is independent in the x and y-axes, and invariant in the z-axis

$$E(x) = -\frac{\Phi_A x}{r_0^2}$$
$$E(y) = \frac{\Phi_A y}{r_0^2} \tag{2}$$

where $E(x)$ and $E(y)$ = electric field strength in the x and y dimensions, Φ_A is the magnitude of the applied potential to the x and y rod pairs, r_0 is the field radius (Fig. 1), and x and y are the displacements from the axis center.

With an applied potential $\Phi_A = (U - V\cos\omega t)/2$, it can be shown that the equations of motion for a positive ion can be defined by the following Mathieu equation [6], where U is the applied dc voltage, V is the peak-to-peak ac voltage, ω is the angular frequency of voltage V, and t is the time:

$$\frac{d^2u}{d\xi^2} + (a_u - 2q_u\cos(2\xi))\,u = 0. \tag{3}$$

The Mathieu parameters a_u and q_u are defined in

$$a_u = a_x = -a_y = \frac{4eU}{m\omega^2 r_0^2} \tag{4}$$

$$q_u = q_x = -q_y = \frac{2eV}{m\omega^2 r_0^2} \tag{5}$$

where e is the charge on the ion, and m is the ion mass.

For a QMF constructed with circular rods of radius r forming a field aperture $r0$ and mounted in a grounded cylindrical enclosure of radius Rc (Fig. 2), an imperfect quadrupole field is generated, which can be represented by a multipole expansion as shown in [18]

$$\Phi(x,y) = \sum_{N=0}^{\infty} \frac{A_N\Phi_N}{r_o^N} \tag{6}$$

$$= \frac{A_0\Phi_0}{r_o^0} + \frac{A_1\Phi_1}{r_o^1} + \frac{A_2\Phi_2}{r_o^2} + \frac{A_3\Phi_3}{r_o^3} + \cdots \tag{7}$$

where A_N is the amplitude of the multipole Φ_N consisting of $2N$ poles, with $A_0\Phi_0$ defining the offset potential, $A_1\Phi_1$ defining the dipole potential, $A_2\Phi_2$ defining the quadrupole potential, $A_3\Phi_3$ defining the hexapole potential, and continuing thereon. For fourfold symmetric QMFs, as considered here, only multipole terms, where $N = 4n + 2$ for $n = 0, 1, 2, 3, \ldots$, contribute to the field.

For the case where fringing effects are not considered, a 2-D field model can be used. Assuming that the x and y fields are independent (uncoupled) for small perturbations of the ion, Newton's second law of motion results in the following two equations defining the x and y trajectory of an ion:

$$m\frac{d^2x}{dt^2} = qE_x \tag{8}$$

$$m\frac{d^2y}{dt^2} = qE_y \tag{9}$$

where $m =$ mass of the ion, q is the charge of the ion, and E_x and E_y are the instantaneous electric field components at the x and y position of the ion.

Computer simulation of ion trajectories in QMFs with hyperbolic rods can be undertaken by a numerical integration of the Mathieu equations. For circular-rod QMFs, it is necessary to solve the field generated by the circular rods for each value of $r/r0$ investigated and then to solve the equations of ion motion for each field. The ion motion, as it traverses the RF field of a QMF, is oscillatory, consisting of a dominant secular oscillation (low frequency) modulated by micromotion (high-frequency oscillation) [21]. The component frequencies are determined by the value of β_x and β_y at the operating point. For zone 1, we use the following equations in obtaining the spatial frequencies:

$$\Omega_{Z1\mu n} = (2n + \beta_\mu)\frac{\omega}{2} \tag{10}$$

where $\Omega_{Z1un} =$ set of secular spatial frequencies for $\mu = x$ or y, $n = 0, 1, 2, 3$ is the frequency ranking, $\beta_\mu = f(a_x, q_x)$ or $f(a_y, q_y)$, and $\omega =$ RF is the excitation angular frequency. For zone 3, the fundamental frequency at the upper stability tip are defined by [22]

$$\Omega_{Z3x} = (2 - \beta_x)\frac{\omega}{2}, \qquad \text{for } 1.5 \le \beta_x < 2 \tag{11}$$

$$\Omega_{Z3y} = \beta_y\frac{\omega}{2}, \qquad 0 \le \beta_y < 0.5. \tag{12}$$

Values of β can be calculated from formulas quoted in Dawson [6] or March and Todd [21] and from published tables. From the ion trajectories (time-domain samples) and by employing the discrete Fourier transform (DFT) [23], the spatial power frequency components can be obtained from

$$X(m) = \sum_{n=0}^{N-1} x(n)e^{-j2\pi nm/N} \tag{13}$$

where $X(m)$ is the mth DFT component, and $x(n)$ is the discrete sequence of time-domain-sampled values.

III. Computer Programs

Custom software (QMS2D-Field) and the public domain computer simulation suite (Poisson/Superfish) [20] were used in these studies. The programs were validated by means of analytical comparison and/or reproduction of previously published experimental or theoretical results. A new ion source generator program (QMS2D-ION), which is based on one that is previously reported [11] and with similar functionality, has been used to generate the entry conditions for a large number of ions ($> 2 \times 10^5$). Ions with a uniform distribution (illumination) across the field aperture and randomly placed with respect to the RF phase were used. Simulation of a hyperbolic-rod QMF was undertaken with the custom program QMS2D-Hyperbolic. This computes individual ion trajectories using a fourth-order Runge–Kutta algorithm to solve the Mathieu equations. The program provides generation, display, and storage of mass spectra and individual ion trajectories, together with parametric sweep control. Poisson/Superfish was used to compute the electric fields for circular-rod QMFs. A geometric model of the QMF was created for each $r/r0$ by the use of primitive text constructs (line and circle), which are stored in a text file together with material definition, electrode potentials, and simulation control settings. The Poisson/Superfish modules (Automesh, Poisson, and SF7) were then used to generate a triangular mesh for the geometric model, to solve the field, and to generate a field file, respectively. A custom utility program extracted the field information and formatted it in a form that is compatible to previously generated field files [11], facilitating validation of the software.

Custom software QMS2D-Field was used to simulate individual ion trajectories within the circular-rod fields. Ion trajectories that are defined by (8) and (9) are solved using a fourth-order Runge–Kutta algorithm. An analytically generated field file for hyperbolic rods was used to validate correct operation and to select a time period increment of sufficient fineness to ensure accurate results. The electric field at an ion position is obtained from the previously generated field files. For ion positions that do not fall at exact grid points, nearest neighbor and bilinear interpolation were used to obtain the exact field value. Other characteristics of the program are similar to QMS2D-Hyperbolic. All custom software was developed under Windows C++.Net 2003 and Visual Studio 2005 for both Windows XP32 and XP64 platforms (copies of the programs are available from the authors).

Ion trajectory power frequency spectra were obtained by simulating a single-ion trajectory and saving the discrete xy coordinates at each step of the trajectory to a file. A custom script was written in MatLab [24], incorporating DFT and PLOT functions, and was used to process the ion trajectory file and generate the power-spatial frequency spectra.

IV. Simulation Methodology

All simulations use 500 steps across the mass range, with 2×10^5 ions traced at each mass step. The QMF control setting $\eta(\text{Res}) = 1$ corresponds to the peak of the stability diagram (i.e., $a_u = 0.23699$ and $q_u = 0.706$ for zone 1). From (4) and (5), assuming hyperbolic rods and introducing η, we obtain

$$\frac{a_u}{q_u} = \eta \frac{2U}{V}. \tag{14}$$

Keeping $q_u = 0.706$ and making $\eta < 1$ moves the operating point below the stability tip, which increases the passband and decreases the resolution. No account of fringing fields at the entrance or exit of the mass filter has been considered, and ion velocity v_z is constant throughout the filter, with ion velocity components $v_x = 0$ and $v_y = 0$ upon entry to the filter. A detected ion occurs if the ions' trajectory does not exceed the field radius over the length of the QMF and when the exit falls within the active area of the detector. Unless otherwise stated, all other test conditions are shown in Table I.

These values have been selected to enable direct comparison with previously reported results [16]. Computed mass spectra for operation in stability zone 1 with circular rods confirm characteristics that are previously reported [16]. Increasing low-mass tail and a shift in mass peak to lower m/z values, with increasing $r/r0$, were reproduced. Also confirmed were variations in peak height and width, increasing transmission, and variations in peak tip shape, as $r/r0$ is altered. Fig. 3 shows a set of spectra for a hyperbolic-rod QMF operating in stability zone 3 for a single-ion species of $40m/z$. No low or high-mass tails on the mass spectral peaks are present, and the rising and falling edges of the peaks are free of artifacts. Transmission through the QMF decreases as control setting η is increased. This reflects a reduction in QMF acceptance, and the inlet aperture is greater than the acceptance for the range of

TABLE I
Computer Simulation Test Conditions

QMF PARAMETER	CONDITION
Length	254 mm
r0	2.76 mm
Frequency	2 MHz
Detector radius	2.76 mm
Housing radius	3.6r0
Ion Source	
Ion energy	2.00 eV
Ion source radius	0.5 mm
Ion energy spread	0
Ion angular spread	0
Operating point	
a (zone 1, zone 3)	0.23699, 3.16
q (zone 1, zone 3)	0.706, 3.23
Ion species	40 m/z

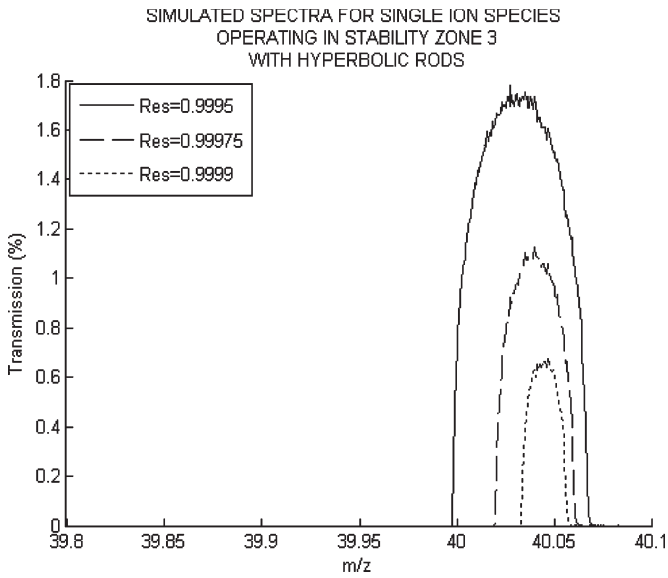

Fig. 3. Simulated zone 3 spectra for Ar^+ ions ($m/z = 40$) for hyperbolic rods.

η considered. A low-amplitude structure is present across the peak tip due to minor changes in the acceptance of the QMF as the mass scan position changes. This is due to the initial phase space positions of a significant number of ions being very close to the QMF acceptance boundary, resulting in small local variations of transmission as the mass scan traverses the mass peak. Increasing the number of ions will reduce these effects, but will result in a corresponding increase in simulation time. Peak tip position shifts to a lower m/z value as the control setting η is decreased due to the asymmetric shape of the $a-q$ diagram about the stability tip.

QMS experimentally obtained mass spectra for $^{59}Co^+$ ions with energy of ~63 eV are shown in Fig. 4, which is derived from [22]. The simulated mass spectra for the QMF section of this instrument, which are obtained using QMS2D-Field, are shown in Fig. 5. Simulated results show very good agreement with the experimental peak, but do contain detailed differences. The low-mass side contains an additional peak. There are detailed differences across the peak tip, with a smaller peak amplitude on the high-mass side. The simulation model

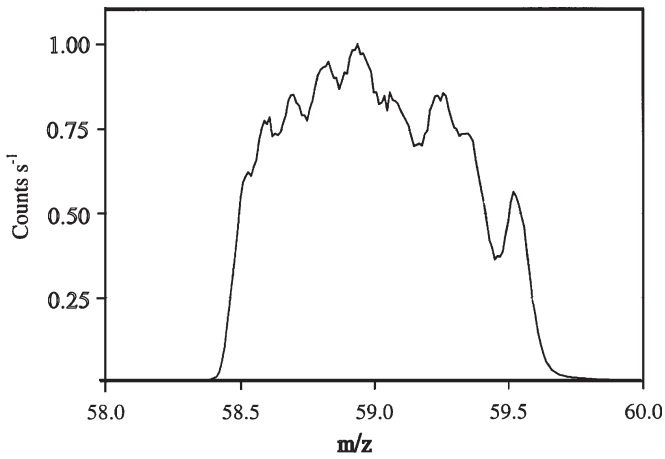

Fig. 4. Zone 3 experimental mass spectra constructed from the data in [22] for $^{59}Co^{+}$ ions with an energy of ∼63 eV.

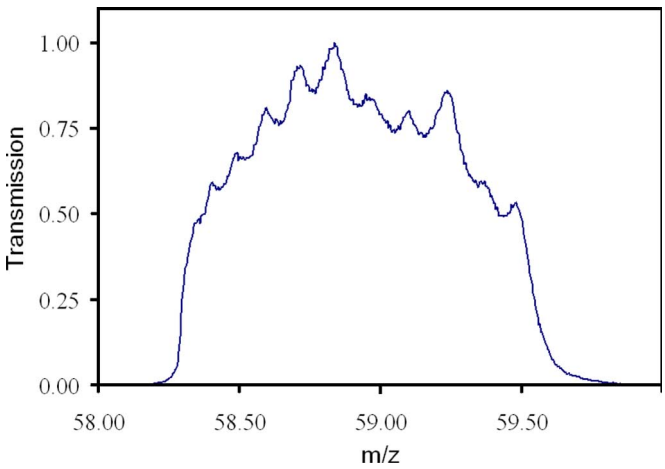

Fig. 5. Zone 3 simulated mass spectra for the QMF [22].

assumed the following: uniform ion source illumination about the centerline, ions enter parallel to the z-axis, no entry or exit fringing fields, parallel rods, and a Faraday cup detector. Similar simulations have shown us that the peak structure is highly dependent on alignment of the ion source and detector, on ion energy spread, and on focusing effects [22]. The exact data on the instrument, operating point, and λ were unavailable, resulting in possible differences between the actual instrument and computational operating conditions. A number of simulations were undertaken, and the presented results reflect the character of the peak shape that is previously reported. Any differences that exist between the two spectra can be attributed to variations in the model and operating point.

Mass spectra for a circular-rod QMF for a range of $r/r0$ ratios when operating in zone 3 ($a \sim 3.16$ and $q \sim 3.23$) are shown in Fig. 6. A number of discernible characteristics are present, which results in a degraded performance when compared to hyperbolic rods. Peak position shifts along the mass scale as $r/r0$ is increased, corresponding to the hyperbolic-rod peak position only when $r/r0 \approx 1.120$. The peak height varies by a factor of three to one for the range of $r/r0$ that is considered, with a minimum occurring at $r/r0 = 1.120$. Peak edges are less sharp due to a broadening of the peak

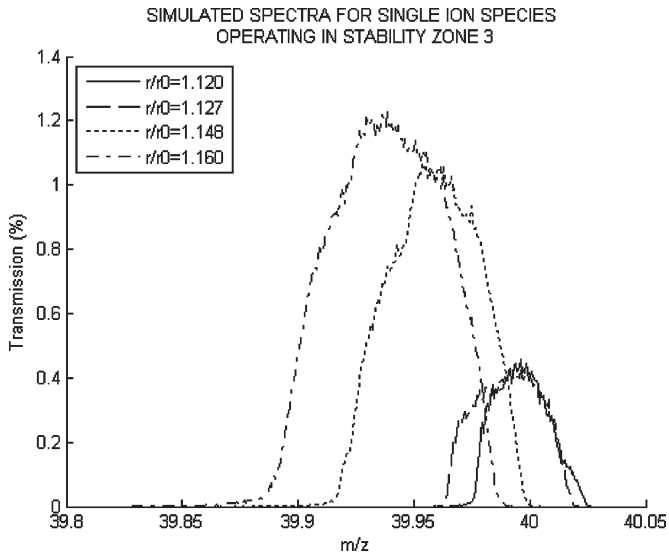

Fig. 6. Simulated spectra for Ar^{+} $(m/z = 40)$ single-ion species operating in stability zone 3.

base, and an increased structure is present across the peak tips. Artifacts are discernible on the low- and high-mass sides, which is more apparent on the low-mass side. Multipole coefficients that are extracted from Poisson show that the dominant quadrupole (A_2) coefficient varies from 1.0009 with $r/r0 = 1.117$ to 1.0037 with $r/r0 = 1.16$. The quadrupole component of the field strength increases as $r/r0$ is increased, resulting in a proportionally higher field strength for a given excitation voltage compared to that generated by hyperbolic rods. This shifts the mass scan line operating point to a lower mass value as $r/r0$ increases. The multipole components in the field result in distortions to the ideal stability diagram. These distortions produce a defocusing of the stability boundaries, with the effect being accentuated near the stability tip (two boundaries converging), which results in a spreading of the transition region between rejection and acceptance. This produces a spreading out of the mass spectral peak base, less steep peak edges, and longer mass spectral tail result. Defocusing near the stability tip also produces an increased structure in the peak (noise) and distortions in peak shape. Fig. 7 shows a set of simulated mass spectral peaks for a range of $r/r0$ at two instrument control settings (η) operating in zone 3. It is evident that a number of mass spectra characteristics are dependent on the value of $r/r0$. Operation at $\eta = 0.9995$ produces nonmonotonic characteristics on the rising edge of the mass peak (greatest at $r/r0 = 1.140$ and reducing either side of this ratio). At $\eta = 0.9999$, these characteristics are not apparent. Similar characteristics are just evident under certain operating conditions on the falling edge (again at $\eta = 0.9995$). For all test conditions, structure is present across the mass peaks, adding uncertainty to the mass peak position. This structure is marginally greater than that observed for hyperbolic rods. Experimental results that are previously reported have demonstrated similar characteristics, including the presence of peak splits [25]. Peak splitting can occur because of misalignment of the ion detector, ion collection effects due to fringing fields at the exit of the QMF coupled with minimum and maximum amplitudes of the ion trajectory

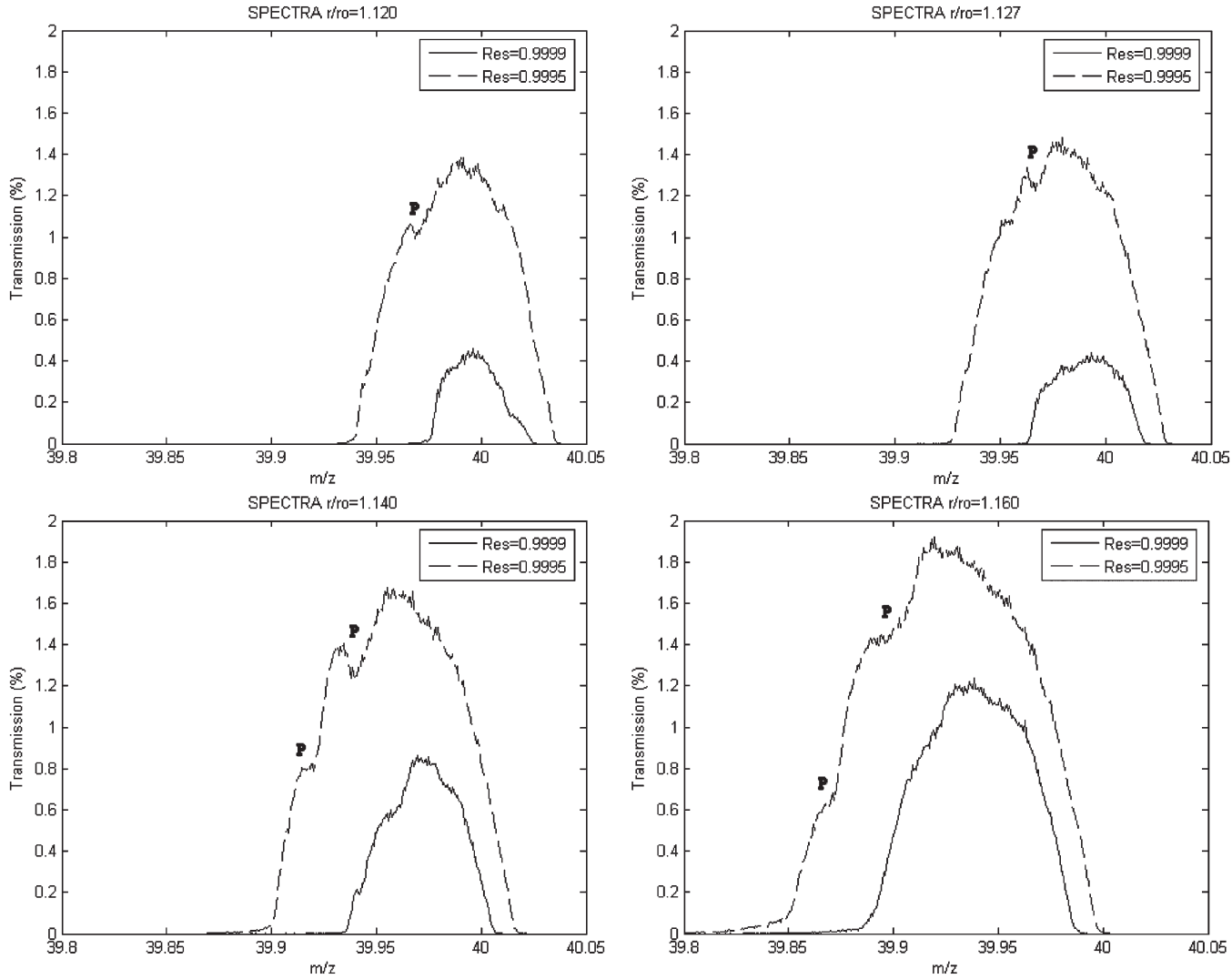

Fig. 7. Set of simulated mass spectra for Ar^+ $(m/z = 40)$ single-ion species operating in stability zone 3 for a range of $r/r0$.

[22], and nonlinear resonances. Simulations were undertaken for a range of ion energies from 2 to 40 eV at $\eta = 0.9995$ for both constant U/V and constant U scanning. For these test conditions, the mass split amplitude (marked as P in Fig. 7) decreased with increasing ion energy, with no measurable shift in the position of the split on the mass scale. As ion energy is increased, ions experience fewer RF cycles, resulting in a reduction in the strength of any nonlinear resonance effects that may be present. These nonlinear resonances are associated with particular lines on the stability diagram, and any characteristics that are associated with these resonances will not shift on the mass scale as ion energy is varied. The observed behavior of the mass peak split Ps conforms to that expected of a mass peak split due to nonlinear resonances in the ion trajectories.

Low-mass tails are present at the two extremes of $r/r0$, with the most pronounced occurring at an $r/r0 = 1.160$ for $\eta = 0.9995$ with an amplitude of $\sim$0.06%, which is insufficient to influence the actual resolution. As $r/r0$ moves away from these two extremes, the low-mass tail reduces, becoming barely detectable at $r/r0 = 1.127$. Zone 3 performance exhibits a marked improvement over zone 1, where extensive low-mass tails were evident, which had a detrimental effect on abundance sensitivity and resolution. Results for zone 3 clearly indicate the improved abundance sensitivity that is obtainable due to the increased baseline peak separation provided by the minimal low-mass tails, and it confirms previously published experimental results [26], [27].

We now introduce a performance sensitivity parameter σ as a method of quantifying the susceptibility of QMF performance parameters to variations in $r/r0$. Peak-height sensitivity σ_{PH} is defined as

$$\sigma_{\mathrm{PH}} = \frac{\delta(\mathrm{PH})}{\delta\left(\frac{r}{r0}\right)} \tag{15}$$

where σ_{PH} is the peak-height sensitivity, PH is the transmission peak height of a mass peak, and $r/r0$ is as previously stated. A range of performance sensitivities can be obtained by suitable substitution of $\delta(\mathrm{PH})$.

Peak-height transmission (Fig. 8) varies with $r/r0$ and is dependent on η. This dependence or performance sensitivity (σ_{PH}) is most marked at the highest setting of η, where peak-height transmission increases by the greatest percentage on either side of a minimum at $r/r0 = 1.120$. At the lowest value

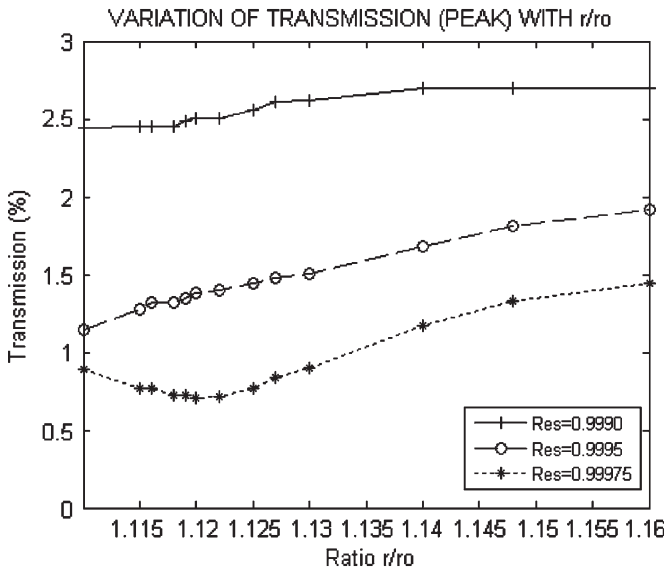

Fig. 8. Variation of transmission (peak height) as a function of $r/r0$ for Ar^+ $(m/z = 40)$ ion.

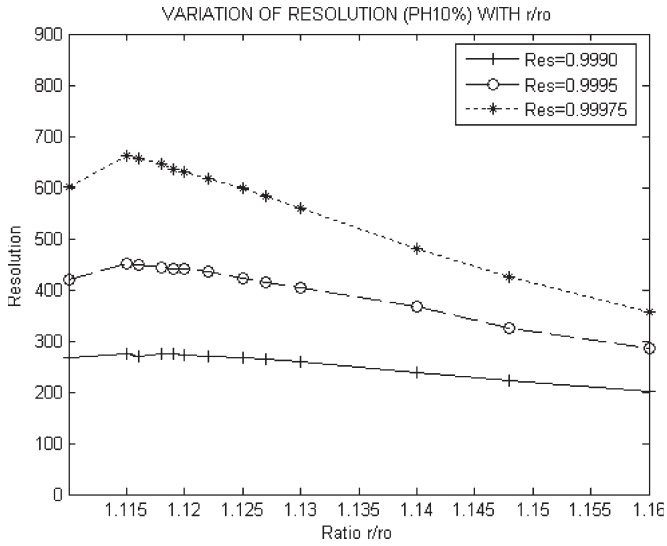

Fig. 9. Variation of resolution (10% PH) as a function of $r/r0$ for Ar^+ $(m/z = 40)$ ion.

of η that is considered, peak height becomes linear, decreasing with increasing $r/r0$, with a lower percentage change and no obvious optimum setting. Performance sensitivity $\sigma_{\rm PH}$ increases as η increases and is dependent on the value of $r/r0$. These results show that QMF acceptance is dependent on $r/r0$, with acceptance staying smaller than the field radius over the tested range.

QMS resolution is determined from the ratio of mass spectral peak width (Δm) at a given mass (m). Resolution $(m/\Delta m)$ is defined, with Δm measured at 10% of the mass spectral peak height (10% PH) or 50% of the peak height (50% PH). The difference between peak heights for the two instrument control settings (η) is greatest at $r/r0 = 1.127$, progressively decreasing on either side as $r/r0$ moves further away from this value. At the higher settings of η, measured resolution (10% and 50% PH) is a maximum for $r/r0 = 1.115{-}1.117$, reducing either side, as shown in Figs. 9 and 10. At lower values

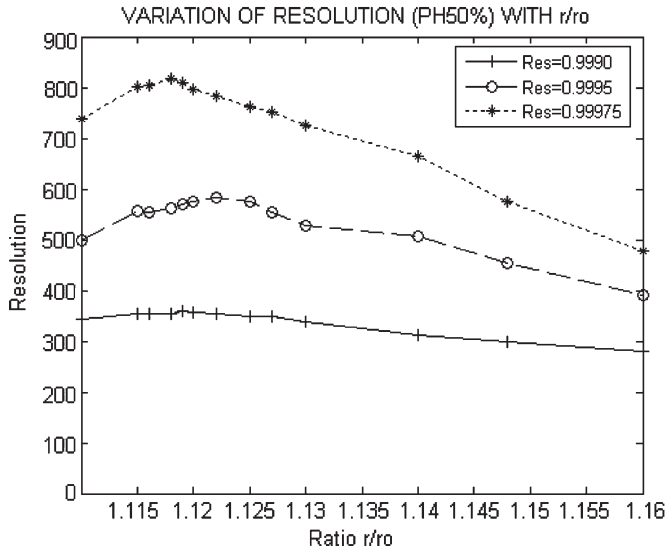

Fig. 10. Variation of resolution (50% PH) as a function of $r/r0$ for Ar^+ $(m/z = 40)$ ion.

of η, the variation of measured resolution is more linear, not indicating any significant optimum value for $r/r0$. Resolution sensitivity for the range of the investigated η is a maximum at $\eta = 0.99975$, demonstrating that performance sensitivity σ_R increases with an increasing η, for the range of η considered.

Peak width exhibits a minimum when $r/r0$ is in the range 1.115–1.122, which is dependent on η and definition (10% or 50% PH). Outside of this range, peak width increases with $r/r0$, with the greatest change for 10% PH. Peak-width sensitivity σ_w is largely independent of η away from the minimum. Mass peak position varies inversely with the $r/r0$ ratio. The absolute value is dependent on resolution, indicating that calibration is required for each control setting (η) of the instrument for zone 3 operation.

Ion transmission magnitude is a function of the vertical distance from the stability tip to the scan line. In the case where the stability tip is defocused, transmission at the peak of the mass spectrum will depend on the degree of defocusing. As the scan line is set closer to the stability peak tip $(\eta \rightarrow 1)$, the contribution from defocusing becomes more significant, resulting in a greater sensitivity to $r/r0$. For an ideal (hyperbolic) field, the intersection points of the scan line with the $a{-}q$ stability diagram define the lower and upper mass pass points and, hence, peak width (Δm). As $r/r0$ moves further from the ideal, the defocusing of the stability boundaries increases with a corresponding increase in Δm.

V. Ion Trajectories

Simulated ion trajectories for zone 1 with hyperbolic rods (Fig. 11) confirm the results that are published in [28]. The x trajectory ion motion consists of a lower frequency approximately sinusoidal waveform which is amplitude modulated to a depth of ≈100% by a much higher frequency. For the y trajectory, ion motion consists of a lower frequency sinusoidal waveform, which is superimposed with a higher frequency component. Zone 3 (Fig. 12) simulated ion trajectories confirm

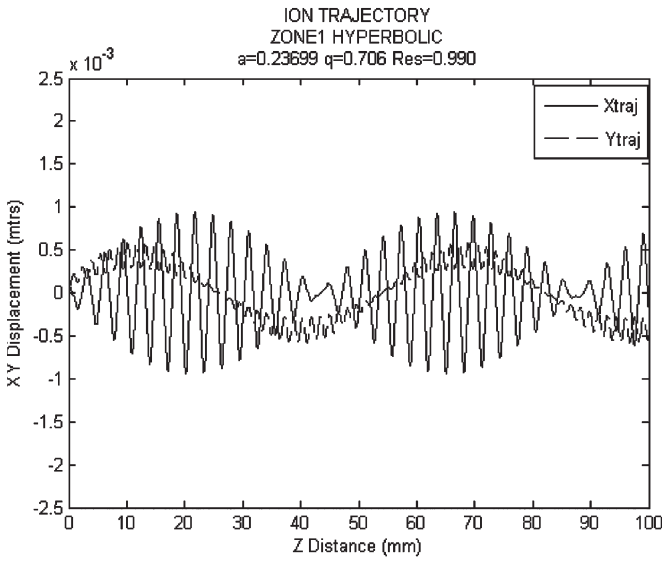

Fig. 11. Zone 1 ion trajectories with hyperbolic rods for Ar^+ $(m/z = 40)$ ion.

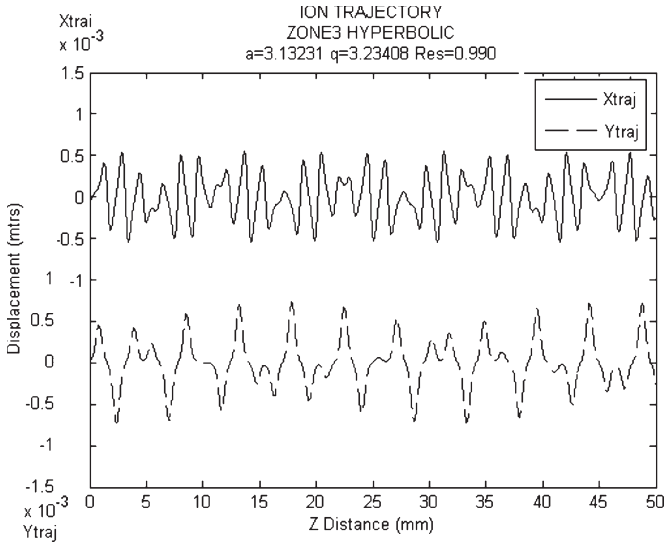

Fig. 12. Zone 3 ion trajectories for hyperbolic rods for Ar^+ $(m/z = 40)$ ion.

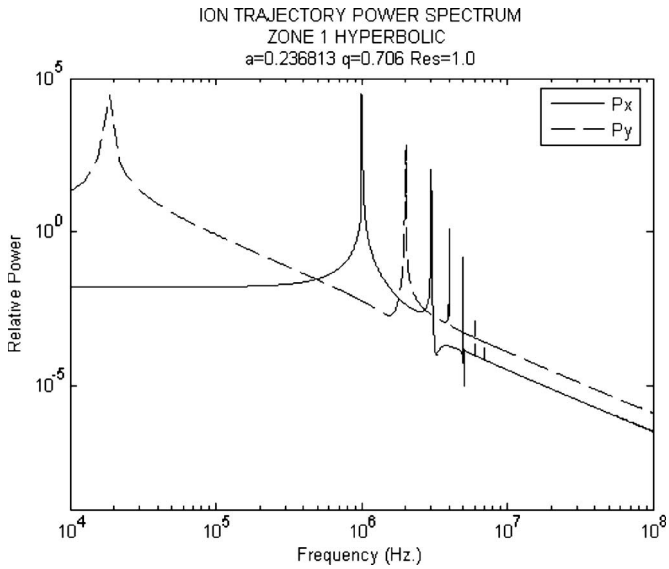

Fig. 13. Zone 1 spatial power frequency spectra for hyperbolic rods for Ar^+ $(m/z = 40)$ ion.

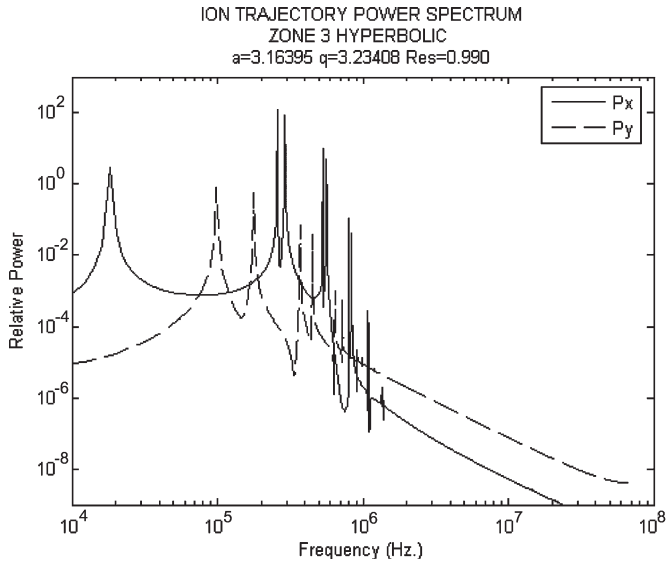

Fig. 14. Zone 3 spatial power frequency spectra for hyperbolic rods for Ar^+ $(m/z = 40)$ ion.

those reported in [29]. For the chosen $a-q$ operating point, they are markedly different to zone 1. Both x and y trajectories have a similar appearance, but with detailed differences. For both axes, the overall appearance is that of a sinusoidal waveform with a large harmonic content.

The ion trajectory power-frequency spectra for zone 1 (Fig. 13) with hyperbolic rods produces dominant x and y-axes spatial frequencies of ~993 and 18 kHz, respectively. At the operating point ($a = 0.236813$ and $q = 0.7060$), the iso-β line values are $\beta_x = 0.988491$ and $\beta_y = 0.0151852$ [27]. The analytically calculated values for the fundamental frequencies using (10) are $\Omega_{Z1x0} = 988.491$ kHz and $\Omega_{Z1y0} = 15.1852$ kHz. These favorably compare with the simulated results. The differences are due to the resolution of the DFT algorithm and simulated data. Higher order spatial frequencies correspond to those obtained through analytical calculation. For both axes, the lowest spatial frequency component exhibits the highest relative power, with each higher order spatial frequency decreasing in relative power. At the selected zone 3 operating point, ion trajectory power spectra display differences from zone 1 (Fig. 14). The lowest spatial frequency now occurs on the x-axis and exhibits a much sharper peak.

The x-axis second-order spatial frequency $(n = 1)$ is now dominant, and for the y-axis, the fundamental spatial frequency $(n = 0)$ is still dominant. A larger number of frequency peaks are apparent, reflecting the less sinusoidal (higher harmonic content) character of zone 3 ion trajectories (Fig. 12).

An analytically derived hyperbolic field was used to validate ion trajectories that are simulated using QMS2D-Field. The obtained trajectories and their associated power frequency spectra very strongly correlated to those obtained by solving the Mathieu equations, demonstrating that field-derived ion trajectories do not introduce significant additional components

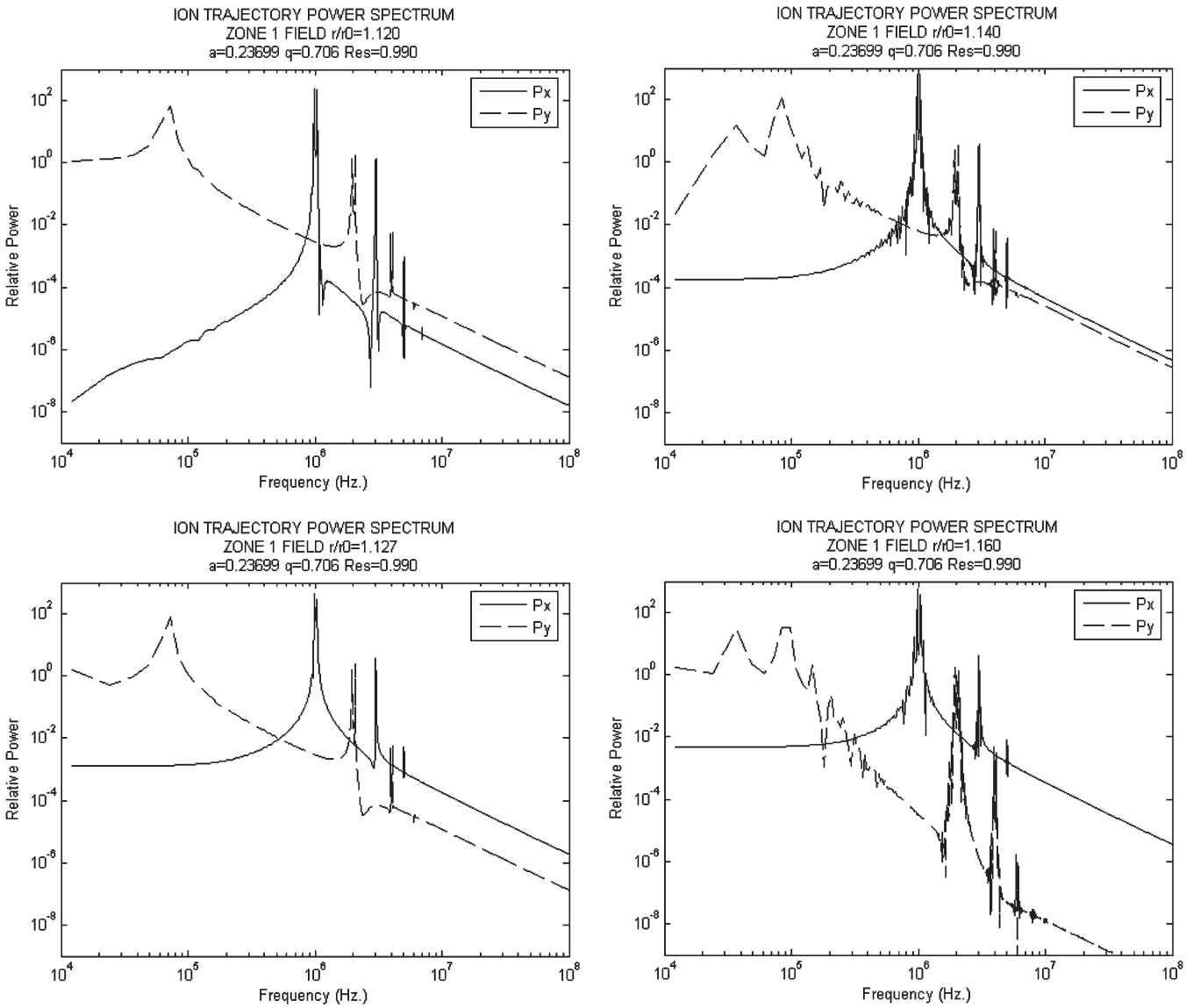

Fig. 15. Set of ion trajectory spatial frequency power spectra for Ar^+ $(m/z = 40)$ ion operating in zone 1 for a range of $r/r0$.

to the power frequency spectra. Ion trajectories for a range of operating conditions and $r/r0$ ratios were simulated. Broadly, they reflect the general characteristics presented for hyperbolic rods. There are certain differences worthy of highlighting. For both zones 1 (Fig. 15) and 3 (Fig. 16), base power levels are increased, which is accompanied by increases in the x and y peak relative powers with increasing $r/r0$. Small changes to the peak frequencies are also discernible. For circular rods, the power spectra are not as clean: there are additional spatial frequency components present. These additional frequency components increase in number and relative power when $r/r0$ further deviates from the accepted optimum of 1.127. This reflects the higher electric field strengths that are inherent with this stability zone compared to zone 1. The power frequency spectra for zone 1 with $r/r0 = 1.127$ show very strong correlation to that obtained for hyperbolic rods. The spatial frequencies are clearly defined, with an absence of the additional spatial frequencies that are present when $r/r0$ is not ideal. Spatial frequencies are very close to those obtained for the hyperbolic electrodes, confirming that the β values are close to those derived from the Mathieu equations. For zone 3, the spatial frequency spectra are not as well defined due to the added clutter of additional spatial frequencies. It is still possible to identify an optimum value for $r/r0$, but there is no strong correlation to the hyperbolic power-spatial frequency spectra. The additional spatial frequency peaks that are observed for circular rods arise from nonlinear resonances occurring due to the nonlinear multipole fields. As $r/r0$ deviates from the ideal, the net effect of these multipole fields varies, resulting in varying nonlinear resonances, which appear as variations in the amplitude and number of spatial frequency peaks that are present in the power-spatial frequency spectra.

VI. Conclusion

The use of a mixture of custom and public domain software has been shown to provide an accurate and efficient simulation method for QMFs. The method allows the use of high-accuracy

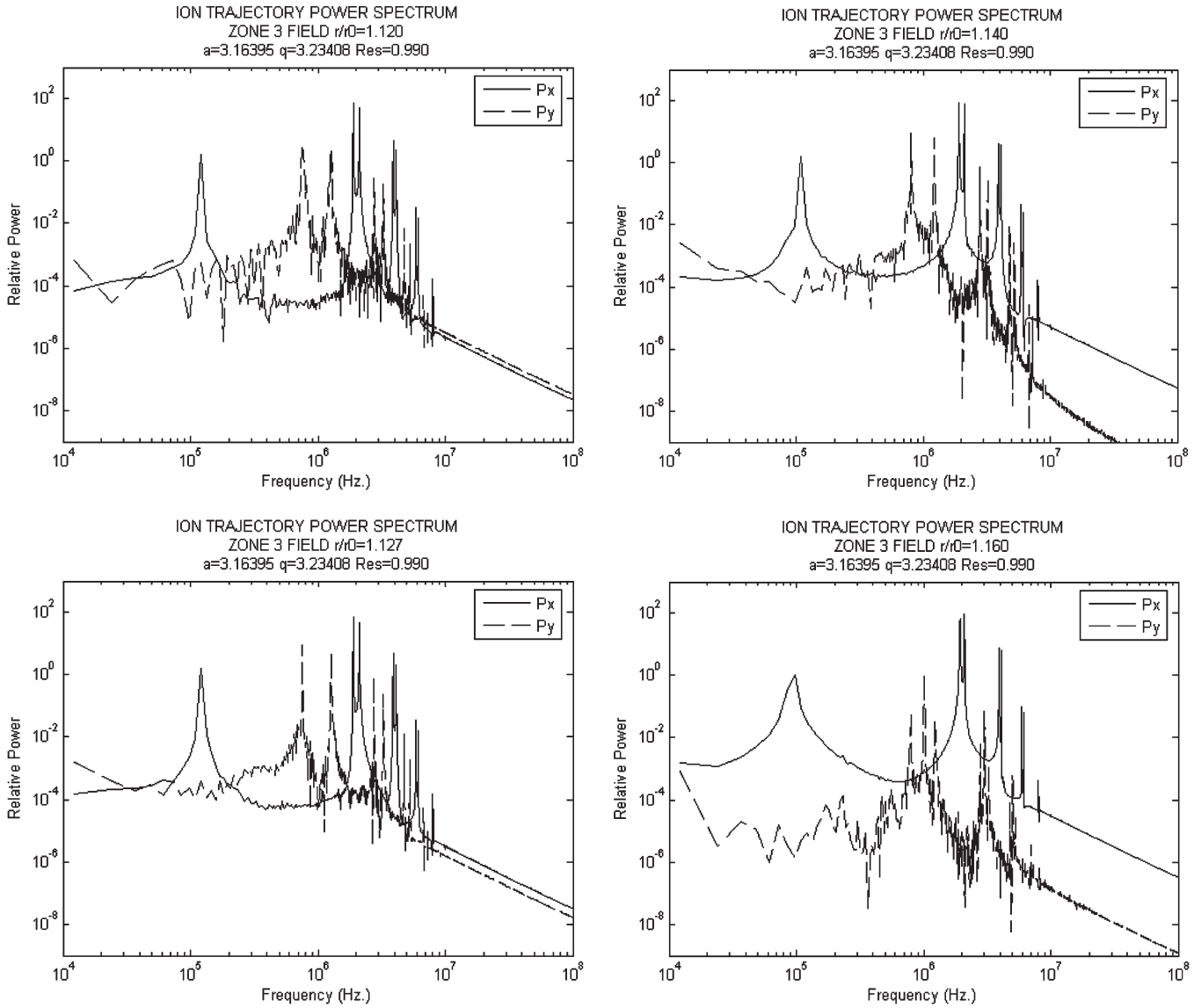

Fig. 16. Set of ion trajectory spatial frequency power spectra for Ar^+ $(m/z = 40)$ ion operating in zone 3 for a range of $r/r0$.

electric field data, which is coupled with the ability to simulate the trajectories of a large number of ions (for each mass spectral peak, 10^8 individual ion trajectories are computed).

QMS operation in zone 3 provides an improved immunity from the effects of the variation in $r/r0$. The increasing mass tails that are apparent when operating in zone 1 are negligible for zone 3, and a very little variation of this feature is apparent with $r/r0$, resulting in a much improved abundance sensitivity for zone 3 over the range of the considered $r/r0$. Artifacts are present in the zone 3 peak shapes, which introduce errors when measuring peak width and height, affecting calculation of the resolution. Similar characteristics are present for zone 1, although at a much reduced level. It is possible that digital-filtering techniques may provide a means of improving these results; a further investigation is recommended. The characteristics of the mass spectra that are obtained demonstrate that circular-rod QMFs result in a shifted and defocused version of the ideal $a-q$ stability diagram. The exact shape and the extent of defocusing are dependent on the ratio of $r/r0$.

The application of the power-spatial frequency DFT techniques allows the effects of the secular and micromotion frequencies of ion trajectories to be quantified. The resultant power-spatial frequency spectra enable the "idealness" of an electric field to be assessed through observation of the presence of additional resonance peaks.

Multipole coefficients and spatial power frequency spectra provide indicators of optimum QMF electrode geometry and can be used to provide a figure of merit (FOM) for a particular geometry under examination. This FOM could act as a controlling variable for an iterative simulation program, enabling automatic generation of the optimum geometry.

ACKNOWLEDGMENT

The authors would like to thank the Department of Electrical Engineering and Electronics, University of Liverpool, for the support and facilities provided; the members of the Quadrupole Mass Spectrometry Group and especially Dr. J. R. Gibson for

his previous research in this field, which provided a foundation for this paper; and LAACG, Los Alamos National Laboratory, for the development of the Poisson Superfish and for making it freely available in the public domain.

REFERENCES

[1] C. Carlberg, I. Bergström, G. Bollen, H. Borgenstrand, R. Jertz, H. J. Kluge, G. Rouleau, R. Schuch, T. Schwarz, L. Schweikhard, P. Senne, and F. Söderberg, "SMILETRAP—A wide-range high-precision mass spectrometer," *IEEE Trans. Instrum. Meas.*, vol. 44, no. 2, pp. 553–557, Apr. 1995.

[2] F. DiFillipo, V. Natarajan, M. Bradley, F. Palmer, S. Rusinkiewicz, and D. E. Pritchard, "Mass spectrometry at 0.1 part per billion for fundamental metrology," *IEEE Trans. Instrum. Meas.*, vol. 44, no. 2, pp. 550–552, Apr. 1995.

[3] R. A. Syms, T. J. Tate, M. M. Ahmed, and S. Taylor, "Design of a micro-engineered electrostatic quadrupole lens," *IEEE Trans. Electron Devices*, vol. 45, no. 11, pp. 2304–2311, Nov. 1998.

[4] S. Taylor, B. Srigengan, J. R. Gibson, D. Tindall, R. Syms, T. Tate, and M. Ahmed, "A miniature mass spectrometer for chemical and biological sensing," in *Proc. SPIE—Int. Soc. Opt. Eng.*, 2000, vol. 4036, pp. 187–193.

[5] E. R. Badman and R. G. Cooks, "Miniature mass analysers," *J. Mass Spectrom.*, vol. 35, pp. 659–671, 2000.

[6] P. H. Dawson, "Principles of operation," in *Quadrupole Mass Spectrometry and Its Applications*. Amsterdam, The Netherlands: Elsevier, 1976, pp. 9–64.

[7] F. M. Ma and S. Taylor, "Simulation of ion trajectories through the mass filter of a quadrupole mass spectrometer," *Proc. Inst. Electr. Eng.—Sci. Meas. Technol.*, vol. 143, no. 1, pp. 71–76, Jan. 1996.

[8] A. C. C. Voo, R. Ng, J. J. Tunstall, and S. Taylor, "Transmission through the quadrupole mass spectrometer mass filter: The effect of aperture and harmonics," *J. Vac. Sci. Technol. A, Vac. Surf. Films*, vol. 15, no. 4, pp. 2276–2281, Jul. 1997.

[9] J. J. Tunstall, A. C. C. Voo, and S. Taylor, "Computer simulation of the mass filter for a finite length quadrupole," *Rapid Commun. Mass Spectrom.*, vol. 11, no. 2, pp. 184–188, 1997.

[10] J. R. Gibson, S. Taylor, and J. H. Leck, "Detailed simulation of mass spectra for quadrupole mass spectrometer systems," *J. Vac. Sci. Technol. A, Vac. Surf. Films*, vol. 18, no. 1, pp. 237–243, Jan. 2000.

[11] J. R. Gibson and S. Taylor, "Prediction of quadrupole mass filter performance for hyperbolic and circular cross section electrodes," *Rapid Commun. Mass Spectrom.*, vol. 14, no. 18, pp. 1669–1673, 2000.

[12] I. E. Dayton, F. C. Shoemaker, and R. F. Mozley, "The measurement of two-dimensional fields Part 2: Study of a quadrupole magnet," *Rev. Sci. Instrum.*, vol. 25, no. 5, pp. 485–489, May 1954.

[13] D. R. Denison, "Operating parameters of a quadrupole in a grounded cylindrical housing," *J. Vac. Sci. Technol.*, vol. 8, no. 1, pp. 266–269, Jan. 1971.

[14] A. J. Reuban, G. B. Smith, P. Moses, A. V. Vagov, M. D. Woods, D. B. Gordon, and R. W. Munn, "Ion trajectories in exactly determined quadrupole fields," *Int. J. Mass Spectrom. Ion Process.*, vol. 154, no. 1/2, pp. 43–59, May 1996.

[15] J. Schulte, P. V. Shevchenko, and A. V. Radchik, "Nonlinear field effects in quadrupole mass filters," *Rev. Sci. Instrum.*, vol. 70, no. 9, pp. 3566–3571, Sep. 1999.

[16] J. R. Gibson and S. Taylor, "Numerical investigation of the effect of electrode size on the behaviour of quadrupole mass filters," *Rapid Commun. Mass Spectrom.*, vol. 15, no. 20, pp. 1960–1964, 2001.

[17] J. R. Gibson and S. Taylor, "Asymmetrical features of mass spectral peaks produced by quadrupole mass filters," *Rapid Commun. Mass Spectrom.*, vol. 17, no. 10, pp. 1051–1055, 2003.

[18] D. J. Douglas and N. V. Konenkov, "Influence of the 6th and 10th spatial harmonics on the peak shape of a quadrupole mass filter with round rods," *Rapid Commun. Mass Spectrom.*, vol. 16, no. 15, pp. 1425–1431, 2002.

[19] P. Turner, S. Taylor, and J. R. Gibson, "The effect of ion entry acceptance conditions on the performance of a quadrupole mass spectrometer operated in upper and lower stability regions," *J. Vac. Sci. Technol. A, Vac. Surf. Films*, vol. 23, no. 3, pp. 480–487, May 2005.

[20] F. L. Krawczyk, J. H. Billen, R. D. Ryne, H. Takeda, and L. M. Young, "The Los Alamos accelerator code group," in *Proc. IEEE Part. Accel. Conf.*, 1995, vol. 4, pp. 2306–2308.

[21] R. E. March and J. F. J. Todd, "Dynamics of ion trapping," in *Quadrupole Ion Trap Mass Spectrometry*, 2nd ed. J. D. Winefordner, Ed. Hoboken, NJ: Wiley, 2005.

[22] Z. Du, J. Douglas, T. Glebova, and N. V. Konenkov, "Peak structure with a quadrupole mass filter operated in the third stability region," *Int. J. Mass Spectrom.*, vol. 197, no. 1–3, pp. 113–121, Feb. 2000.

[23] R. G. Lyons, "The discrete Fourier transform," in *Understanding Digital Signal Processing*. Reading, MA: Addison-Wesley, 1996.

[24] The Mathworks Inc., *MatLab*. [Online]. Available: www.mathworks.com

[25] S. Hiroki, T. Abe, and Y. Murakam, "Development of a quadrupole mass spectrometer using the second stable zone in Mathieu's stability diagram," *Rev. Sci. Instrum.*, vol. 62, no. 9, pp. 2121–2124, Sep. 1991.

[26] Z. Du, T. N. Olney, and D. J. Douglas, "Inductively coupled plasma mass spectrometry with a quadrupole mass filter operated in the third stability region," *J. Amer. Soc. Mass Spectrom.*, vol. 8, no. 12, pp. 1230–1236, Dec. 1997.

[27] S. Hiroki, T. Ebe, and Y. Murakami, "Separation of helium and deuterium peaks with a quadrupole mass spectrometer by using the second stability zone in the Mathieu diagram," *Rev. Sci. Instrum.*, vol. 63, no. 8, pp. 3874–3876, Aug. 1992.

[28] J. H. Batey, "Quadrupole gas analysers," *Vacuum*, vol. 37, no. 8/9, pp. 659–668, 1987.

[29] M. Y. Sudakov, "Spectrum of charged particle oscillations in an RF quadrupole field," *Tech. Phys.*, vol. 45, no. 3, pp. 322–329, Mar. 2000.

Thomas J. Hogan obtained the qualifications for Chartered Engineer (electrical and electronic) in 1971 from Hendon College of Technology (now Middlesex University), London, U.K., and received the M.Sc. degree in microelectronics (with distinction) from the University of Bolton, Bolton, U.K. and the University of Northumbria, Newcastle, U.K., in 2004. He is currently an external student with the Department of Electrical Engineering and Electronics, University of Liverpool, Liverpool, U.K.

He is an independent Consultant Engineer in Cambridge, U.K., and has acted for organizations such as the DTI, BAe, and Thales on the design of bespoke electronic and software systems, including computer graphics, satellite imaging, scientific instrumentation, and laser systems. His professional interests include instrumentation, automotive, and embedded control. His research interests include numerical simulation, instrumentation, and reversible computing.

Mr. Hogan is a European Engineer and a member of the Institute of Engineering & Technology, U.K.

Stephen Taylor received the B.Sc. degree from Imperial College, London, U.K., in 1978 and the M.Eng. and Ph.D. degrees from the University of Liverpool, Liverpool, U.K., in 1983 and 1988, respectively.

He is currently a Reader with the Department of Electrical Engineering and Electronics, University of Liverpool, where he teaches electromagnetics and MEMS design. He has acted as a Consultant to several U.K. companies and is a Director of a University spinout company. He is the Author or Coauthor of over 165 articles, patents, or publications in the scientific literature. In 1995, he invented and codeveloped the (then) world's smallest mass spectrometer, which was the first one to be microengineered in silicon. His research interests include nanotechnology and quantum information processing using ion traps.

Dr. Taylor is a Chartered Engineer and a Fellow of the Institute of Engineering & Technology, U.K. He is a member of the program committee of the Harsh Environment Mass Spectrometry Conference and a former member of the committee for the IEEE Semiconductor Interface Specialist Conference.